ChemComm

COMMUNICATION

View Article Online
View Journal | View Issue

Cite this: *Chem. Commun.*, 2023, **59**, 732

Received 28th September 2022,
Accepted 3rd December 2022

DOI: 10.1039/d2cc05314d

rsc.li/chemcomm

Formation of a meltable purinate metal–organic framework and its glass analogue†

Alice M. Bumstead,[a] Celia Castillo-Blas,[a] Ignas Pakamorė,[b] Michael F. Thorne,[a] Adam F. Sapnik,[a] Ashleigh M. Chester,[a] Georgina Robertson,[a] Daniel J. M. Irving,[c] Philip A. Chater,[c] David A. Keen,[d] Ross S. Forgan[b] and Thomas D. Bennett*[a]

The chemistries that can be incorporated within melt-quenched zeolitic imidazolate framework (ZIF) glasses are currently limited. Here we describe the preparation of a previously unknown purine-containing ZIF which we name ZIF-UC-7. We find that it melts and forms a glass at one of the lowest temperatures reported for 3D hybrid frameworks.

Metal–organic frameworks (MOFs) are a widely studied family of porous materials composed of inorganic nodes and organic molecular linkers.[1,2] Interest in these materials has increased in recent years due to their wide variety of potential applications encompassing heterogeneous catalysis,[3,4] gas storage and separation,[5,6] and biomedicine.[7,8]

Zeolitic imidazolate frameworks (ZIFs) are a subset of MOFs composed of tetrahedrally coordinated M^{2+} metal nodes connected to imidazolate linkers that are well known for their high thermal and chemical stabilities.[9,10] Recently, it has been demonstrated that certain ZIFs can melt.[11] Quenching these materials from the liquid state results in the preparation of melt-quenched MOF glasses—the first new category of glass reported in 50 years.[12,13]

Melting in ZIFs is a dynamic process, involving rapid de-coordination and re-coordination of the imidazolate linkers.[11] However, even though more than one hundred ZIF structures have been reported,[14] only a handful of ZIFs have been found to form melt-quenched glasses.[12,13] The most well-studied glass-forming ZIF is ZIF-62 $[Zn(Im)_{2-x}(bIm)_x]$ (Im – imidazolate – $C_3H_3N_2^-$) (bIm – benzimidazolate – $C_7H_5N_2^-$) which crystallises in the *Pbca* space group and displays the **cag** network topology.[15–17] Various studies have demonstrated that it is possible to alter the melting behaviour of ZIF-62 by changing the metal cation from Zn^{2+} to Co^{2+}, as well as by altering the ratio of Im to bIm in the structure.[18–20] Other **cag** topology ZIFs have since been shown to melt, with different functionalised bIm linkers incorporated to alter their thermal behaviour.[21–23] However, the incorporation of other organic linker chemistries into glass-forming ZIFs has yet to be reported.

The use of MOFs in biomedical applications is gaining increasing interest due to their tuneable pore sizes and varied chemistry.[7] For these applications, it is essential that MOFs contain biocompatible metal ions such as Zr^{4+}, Zn^{2+} or Fe^{2+},[8,24] and biocompatible organic linkers such as amino acids, peptides, carbohydrates and nucleobases.[25–27] Various MOFs have been prepared using the nucleobase adenine as an organic linker and these frameworks have shown promise for CO_2 uptake, heterogeneous catalysis and drug delivery.[28–30] Adenine is part of the family of molecules known as purines, the simplest of these being purine itself. Purine has already been incorporated as an organic component in various ZIFs,[31–33] however, the thermal behaviour of purine-containing ZIFs has not been explored in detail.

It is not only MOFs that have been proposed for biomedical applications. Inorganic glasses, including phosphates and borates, are promising candidates for biomedical applications including drug delivery and bone tissue regeneration.[34,35] Given the promise of both crystalline MOFs and inorganic glasses in biomedicine, the motivation of this study was to see how biological functionality may be incorporated into a MOF glass. Here we describe the preparation of a previously unknown purine-containing ZIF, denoted ZIF-UC-7 (Fig. 1), before demonstrating its melting and glass-forming behaviour.

Solvothermal synthesis was used to prepare orange single crystals of ZIF-UC-7 (Methods and Fig. S1, S2, ESI†). Specifically, zinc nitrate hexahydrate (5.09 mmol), imidazole (108 mmol) and purine (12.0 mmol) were dissolved in *N*,*N*-dimethylformamide

[a] *Department of Materials Science and Metallurgy, University of Cambridge, Cambridge, CB3 0FS, UK. E-mail: tdb35@cam.ac.uk*
[b] *WestCHEM, School of Chemistry, The University of Glasgow, University Avenue, Glasgow, G12 8QQ, UK*
[c] *Diamond Light Source Ltd, Diamond House, Harwell Campus, Didcot, Oxfordshire, OX11 0DE, UK*
[d] *ISIS Facility, Rutherford Appleton Laboratory, Harwell Campus, Didcot, Oxfordshire, OX11 0QX, UK*

† Electronic supplementary information (ESI) available. CCDC 2209865. For ESI and crystallographic data in CIF or other electronic format see DOI: https://doi.org/10.1039/d2cc05314d

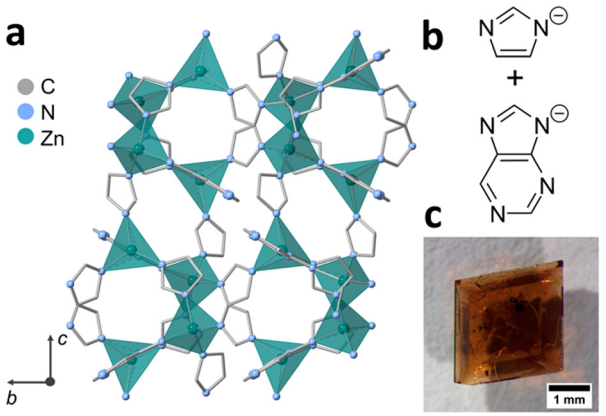

Fig. 1 (a) Crystal structure of **cag** topology ZIF-UC-7 viewed down the crystallographic *a* axis. Atoms shown are carbon – grey, nitrogen – blue and zinc – green. Hydrogen atoms and disorder from multiple linker occupancy have been omitted for clarity. (b) Imidazolate and purinate linkers found in the structure. (c) Optical image of a single crystal of ZIF-UC-7.

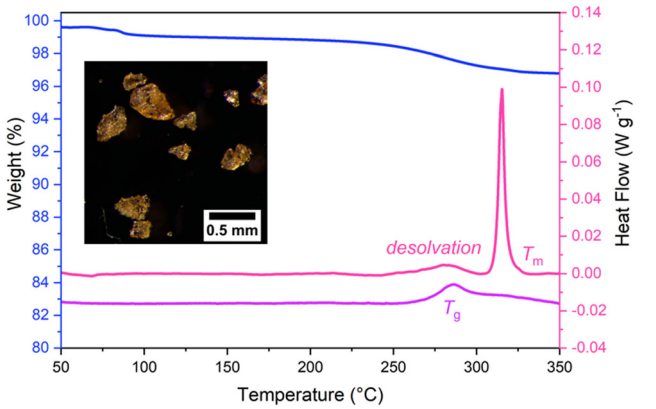

Fig. 2 TGA trace (blue) and DSC traces (1st upscan – pink, 2nd upscan – purple) of ZIF-UC-7 between 50 and 350 °C. Heat flow direction: endo – up. T_m was taken as the offset of the melting endotherm, with T_m = 318 °C. T_g was taken as the mid-point of the glass transition, with T_g = 273 °C. Inset: Optical image of pieces of ZIF-UC-7 glass, denoted a_gZIF-UC-7.

(DMF), heated to 130 °C and held there for 48 h. Single crystal X-ray diffraction (SCXRD) established their crystallisation in the *Pbca* space group (a = 15.1336(5) Å, b = 15.4532(5) Å, c = 18.4151(6) Å, V = 4306.6(2) Å^3) (Fig. 1 and Table S1, ESI†). ZIF-UC-7 therefore crystallises with a very similar unit cell to many liquid and glass-forming ZIFs.[18,36] The purinate ligand (pur – $C_5H_3N_4^-$) is located on only one of the four possible linker positions in 1 : 1 occupational disorder with an imidazolate ligand, resulting in a composition of $[Zn(Im)_{1.75}(pur)_{0.25}]$. The half-occupied purine site is itself disordered across two orientations in a 3 : 1 ratio. A powder sample was then prepared by ball-milling these crystals at 20 Hz for five minutes (Methods and Fig. S3–S5, Table S2, ESI†). Solution state ^{1}H NMR spectroscopy (Fig. S6, ESI†) confirmed the composition of the bulk powder to be $[Zn(Im)_{1.75}(pur)_{0.25}]$, in agreement with the composition determined by SCXRD.

The thermal behaviour of ZIF-UC-7 was then studied in detail (Fig. 2). Thermogravimetric analysis (TGA) revealed that thermal decomposition began above T_d = 550 °C (Fig. S7, ESI†). Differential scanning calorimetry (DSC) was then used to locate a melting endotherm (T_m = 318 °C) which was lower than the onset of thermal decomposition (Fig. S8, ESI†). However, these measurements displayed a second, broad endotherm which obscured the melting event (Fig. S8, ESI†). Assessment of the TGA trace revealed that melting was accompanied by a *ca.* 3% mass loss (Fig. S7, ESI†). Furthermore, solution state ^{1}H NMR spectroscopy revealed that DMF was present in the ZIF (Fig. S6, ESI†), despite the rigorous washing and activation procedure used (Methods). The broad feature in the DSC is therefore attributed to the release of DMF from the framework during heating. ^{1}H NMR spectroscopy and CHN microanalysis of a sample of ZIF-UC-7 heated to 400 °C then confirmed this DMF can be thermally removed (Fig. S9 and Tables S3, S4, ESI†).

An *in situ* activation procedure was then performed in the DSC instrument to isolate the melting endotherm (Fig. S10, ESI†). First, a sample of ZIF-UC-7 was held at 275 °C under an argon atmosphere for five minutes to remove excess DMF from the structure (Fig. S11 and Table S5, ESI†). This pre-heated sample was cooled to 30 °C before heating to 350 °C to observe the unobscured melting event (T_m = 318 °C) (Fig. 2 and Fig. S12, ESI†). Finally, this sample was cooled to 30 °C before heating a third time to locate its glass transition (T_g = 273 °C) (Fig. 2 and Fig. S12, ESI†), *i.e.*, the temperature where the glass transforms to a more flowable, liquid-like state. Hereafter, samples of ZIF-UC-7 melt-quenched from above T_m will be denoted a_gZIF-UC-7.

^{1}H NMR spectroscopy confirmed that a_gZIF-UC-7 has the same composition as crystalline ZIF-UC-7, *i.e.*, $[Zn(Im)_{1.75}(pur)_{0.25}]$, with no decomposition observed until 340 °C (Fig. S13, ESI†). Moreover, only diffuse scattering was observed in its X-ray diffraction pattern (Fig. S3, ESI†), supporting its transformation to the glass phase. Furthermore, particle coalescence and sample flow were evident from optical microscopy and scanning electron microscopy (SEM) (Fig. 2, 3 and Fig. S15, ESI†).

The melting event was then investigated further by heating separate samples of ZIF-UC-7 to 250 °C, 275 °C, 305 °C, 315 °C, 350 °C, 400 °C and 450 °C followed by *ex situ* powder X-ray diffraction (PXRD) (Fig. S16, ESI†). Bragg reflections from ZIF-UC-7

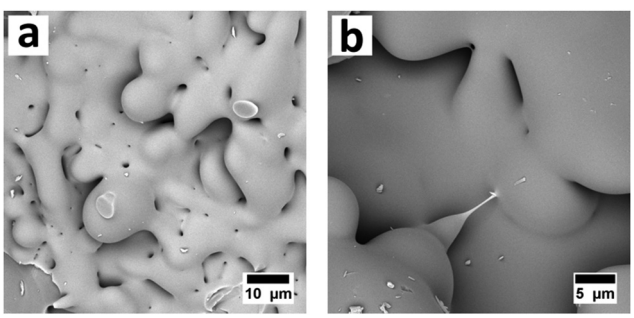

Fig. 3 SEM images at (a) 10 μm and (b) 5 μm magnification, of a_gZIF-UC-7 after quenching from 350 °C. Vitreous flow and bubble formation are evident, supporting transformation to the glass phase.

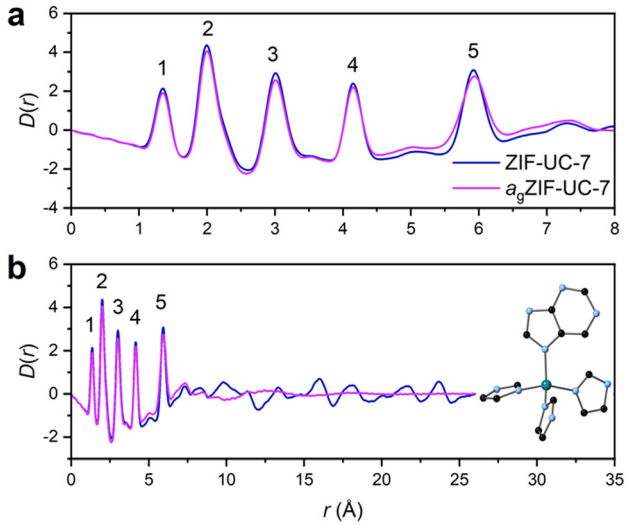

Fig. 4 PDFs of ZIF-UC-7 (blue) and a_gZIF-UC-7 (purple). (a) $D(r)$ between 0 and 8 Å, highlighting the similarities in local structure between ZIF-UC-7 and a_gZIF-UC-7. (b) $D(r)$ between 0 and 25 Å, illustrating the lack of long-range order (correlations > 8 Å) in a_gZIF-UC-7. Inset: Zn^{2+} ion coordinated to three Im linkers and one pur linker. Atoms shown are carbon – black, nitrogen – blue and zinc – green. The five dominant correlations at low r are labelled (1–5).

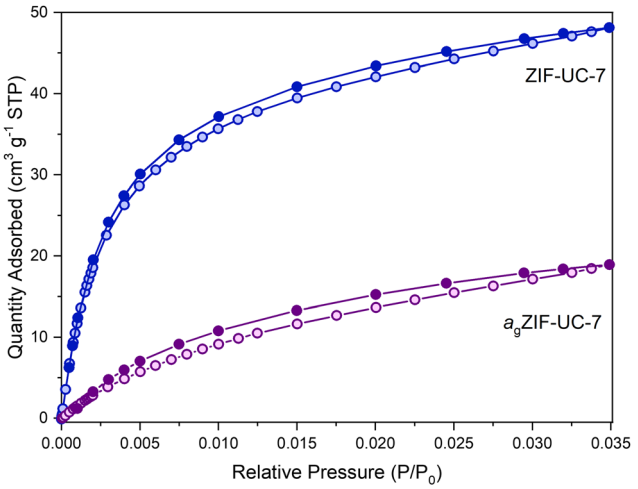

Fig. 5 CO_2 sorption isotherms for ZIF-UC-7 (blue) and a_gZIF-UC-7 (purple). ZIF-UC-7 displayed a maximum CO_2 uptake of 48.1 cm^3 g^{-1}. a_gZIF-UC-7 exhibited a lower maximum uptake of 18.9 cm^3 g^{-1}. Adsorption isotherms represented by open circles. Desorption isotherms represented by closed circles.

were observed for samples heated to temperatures below 305 °C. However, for samples heated above this temperature, all reflections were lost, and only diffuse scattering was observed. ZIF-UC-7 therefore displays a large working temperature range for a ZIF (*i.e.*, the temperature range between T_m and T_d, Table S7).[12]

The structure of a_gZIF-UC-7 was then compared to that of crystalline ZIF-UC-7 using X-ray total scattering data collected at beamline I15-1 at the Diamond Light Source (Fig. S17, ESI†). Fourier transformation of the corrected total scattering data yielded their pair distribution functions (PDFs) (Fig. 4). The local structure of a_gZIF-UC-7 was similar to that of ZIF-UC-7. Both materials displayed the same short-range order correlations (labelled 1–5). Correlations 1 to 5 were dominated by C═C/C–N, Zn–N, Zn···C, Zn···N and Zn···Zn distances, in turn, which is very similar to ZIF-62.[37] However, the change in linker chemistry from bIm to pur (*i.e.*, the replacement of two C atoms with N atoms) will lead to a marginal increase in weighting for all *N*-containing partial PDFs within the total PDF. Furthermore, the static disorder for both the Im and pur linkers will result in slight peak broadening due to the presence of different configurations. Nevertheless, the lack of distinct correlations over longer distances in a_gZIF-UC-7 confirms its transformation to the glass phase.

CO_2 sorption isotherms were then collected at 273 K for both crystalline ZIF-UC-7 and a_gZIF-UC-7 (Fig. 5). ZIF-UC-7 has a maximum CO_2 uptake of 48.1 cm^3 g^{-1} (Fig. S18 and Table S8, ESI†). This is comparable to the CO_2 uptake reported for other glass-forming ZIFs[21,22] and approaches some of the highest values of CO_2 uptake reported to date with a **cag** topology (Table S9, ESI†).[10,38] This high CO_2 uptake is likely due to the large number of nitrogen atoms in the framework from the purinate linker, as nitrogen atoms have previously been shown to have a high affinity for Lewis acidic gases such as CO_2.[5]

As expected, a_gZIF-UC-7 has a lower CO_2 uptake (18.9 cm^3 g^{-1}) (Fig. S19 and Table S10, ESI†) due to the pore network collapsing upon glass formation. This value is similar to the uptake values of other glassy ZIFs.[22] However, although glass formation results in a reduction in CO_2 uptake, it does not completely preclude framework porosity.

ZIF-UC-7 displays one of the lowest T_m values recorded for a ZIF.[13] To rationalise this behaviour, the enthalpic (ΔH_{fus}) and entropic (ΔS_{fus}) contributions to melting were calculated based on reported methods[39] and compared to values calculated for other ZIFs (Fig. S20 and Table S7, ESI†).[22,36] Of all these systems, ZIF-UC-7 had the lowest value for ΔH_{fus}, where lower ΔH_{fus} values result in a reduced T_m.[39] Therefore, as has been found for other ZIFs,[22] the low T_m of ZIF-UC-7 may result from an enthalpic effect, such as weaker Zn–N coordination bonds in the framework. However, other factors may also be contributing to the low T_m of ZIF-UC-7. For example, during melting the uncoordinated, recently detached, purinate ion may be more stable than an equivalent benzimidazolate ion, as the negative charge can be delocalised across four nitrogen atoms in the purinate ion. A more stable uncoordinated linker could potentially lower the energy barrier for the dissociative melting mechanism, resulting in a reduction in T_m. In addition, the purinate linker contains additional N donor atoms. These may act as additional transient coordination sites during melting, helping to stabilise the uncoordinated linkers that form during the melting process. Regardless of the factors contributing to melting, the T_m of ZIF-UC-7 is remarkably low compared to other ZIFs, which may be advantageous for material processing.

The T_g for a_gZIF-UC-7 (T_g = 273 °C) is also one of the lowest values reported for a ZIF.[13,20] This may also be attributed to an enthalpic effect, such as weaker coordination bonds in the

framework.[39] Additionally, the smaller size of the purinate linker (steric index *ca.* 618 Å^4) compared to a substituted benzimidazolate linker (steric index *ca.* 915 Å^4) may result in an increase in steric freedom in the glass and hence a reduction in T_g.[12,40,41] The use of purinate linkers in ZIFs and their glasses is therefore a promising strategy to lower both T_m and T_g.

To conclude, in this work we have expanded the types of possible molecules that can be incorporated within MOF glasses by the successful inclusion of purine in ZIF-UC-7. Moreover, the presence of the purinate linker in ZIF-UC-7 results in ZIF-UC-7 displaying one of the lowest melting temperatures (T_m = 318 °C) and glass transition temperatures (T_g = 273 °C) reported for any ZIF. Furthermore, its successful incorporation in a ZIF glass provides a promising case study, illustrating how biologically active purines, including nucleobases such as adenine and guanine, may be incorporated within ZIF glasses.

A. M. B. and M. F. T. conceptualised the project. A. M. B. synthesised and characterised all samples. I. P. and R. S. F. collected the SCXRD data and performed the structural refinement. C. C. B. and A. M. B. collected the SEM images and gas sorption data. C. C. B., A. F. S., A. M. C., G. R., D. J. M. I., P. C., and D. A. K. collected the total scattering data. A. M. B. and D. A. K. processed the total scattering data. M. F. T. and A. F. S. contributed useful discussions. T. D. B. supervised the project and acquired funding. A. M. B. wrote the manuscript and all authors contributed to the final version.

Conflicts of interest

There are no conflicts to declare.

References

1 H. Furukawa, K. E. Cordova, M. O'Keeffe and O. M. Yaghi, *Science*, 2013, **641**, 1230444.
2 H. C. Zhou and S. Kitagawa, *Chem. Soc. Rev.*, 2014, **43**, 5415–5418.
3 L. Zhu, X. Q. Liu, H. L. Jiang and L. B. Sun, *Chem. Rev.*, 2017, **117**, 8129–8176.
4 D. Yang and B. C. Gates, *ACS Catal.*, 2019, **9**, 1779–1798.
5 K. Sumida, D. L. Rogow, J. A. Mason, T. M. McDonald, E. D. Bloch, Z. R. Herm, T. H. Bae and J. R. Long, *Chem. Rev.*, 2012, **112**, 724–781.
6 E. D. Bloch, W. L. Queen, R. Krishna, J. M. Zadrozny, C. M. Brown and J. R. Long, *Science*, 2012, **335**, 1606–1610.
7 A. C. McKinlay, R. E. Morris, P. Horcajada, G. Férey, R. Gref, P. Couvreur and C. Serre, *Angew. Chem., Int. Ed.*, 2010, **49**, 6260–6266.
8 P. Horcajada, R. Gref, T. Baati, P. K. Allan, G. Maurin, P. Couvreur, G. Férey, R. E. Morris and C. Serre, *Chem. Rev.*, 2012, **112**, 1232–1268.
9 K. S. Park, Z. Ni, A. P. Cote, J. Y. Choi, R. Huang, F. J. Uribe-Romo, H. K. Chae, M. O'Keeffe and O. M. Yaghi, *Proc. Natl. Acad. Sci. U. S. A.*, 2006, **103**, 10186–10191.
10 A. Phan, C. J. Doonan, F. J. Uribe-Romo, C. B. Knobler, M. O. Keeffe and O. M. Yaghi, *Acc. Chem. Res.*, 2010, **43**, 58–67.
11 R. Gaillac, P. Pullumbi, K. A. Beyer, K. Chapman, D. A. Keen, T. D. Bennett and F. X. Coudert, *Nat. Mater.*, 2017, **16**, 1149–1154.
12 T. D. Bennett and S. Horike, *Nat. Rev. Mater.*, 2018, **3**, 431–440.
13 N. Ma and S. Horike, *Chem. Rev.*, 2022, **122**, 4163–4203.
14 K. Noh, J. Lee and J. Kim, *Isr. J. Chem.*, 2018, **58**, 1075–1088.
15 R. Banerjee, A. Phan, B. Wang, C. Knobler, H. Furukawa, M. O'Keeffe and O. M. Yaghi, *Science*, 2008, **319**, 939–943.
16 R. S. K. Madsen, A. Qiao, J. Sen, I. Hung, K. Chen, Z. Gan, S. Sen and Y. Yue, *Science*, 2020, **367**, 1473–1476.
17 Y. Wang, H. Jin, Q. Ma, K. Mo, H. Mao, A. Feldhoff, X. Cao, Y. Li, F. Pan and Z. Jiang, *Angew. Chem.*, 2020, **132**, 4395–4399.
18 L. Frentzel-Beyme, M. Kloß, R. Pallach, S. Salamon, H. Moldenhauer, J. Landers, H. Wende, J. Debus and S. Henke, *J. Mater. Chem. A*, 2019, **7**, 985–990.
19 M. F. Thorne, M. L. Rios Gomez, A. M. Bumstead, S. Li and T. D. Bennett, *Green Chem.*, 2020, **22**, 2505–2512.
20 L. Frentzel-Beyme, M. Kloß, P. Kolodzeiski, R. Pallach and S. Henke, *J. Am. Chem. Soc.*, 2019, **141**, 12362–12371.
21 J. Hou, M. L. Ríos Gómez, A. Krajnc, A. McCaul, S. Li, A. M. Bumstead, A. F. Sapnik, Z. Deng, R. Lin, P. A. Chater, D. S. Keeble, D. A. Keen, D. Appadoo, B. Chan, V. Chen, G. Mali and T. D. Bennett, *J. Am. Chem. Soc.*, 2020, **142**, 3880–3890.
22 A. M. Bumstead, I. Pakamorė, K. D. Richards, M. F. Thorne, S. S. Boyadjieva, L. N. McHugh, A. F. Sapnik, D. S. Keeble, D. A. Keen, R. C. Evans, R. S. Forgan and T. D. Bennett, *Chem. Mater.*, 2022, **34**, 2187–2196.
23 R. S. K. Madsen, S. Sarkar, B. B. Iversen and Y. Yue, *Chem. Commun.*, 2022, **58**, 823–826.
24 I. Abánades Lázaro and R. S. Forgan, *Coord. Chem. Rev.*, 2019, **380**, 230–259.
25 R. A. Smaldone, R. S. Forgan, H. Furukawa, J. J. Gassensmith, A. M. Z. Slawin, O. M. Yaghi and J. F. Stoddart, *Angew. Chem., Int. Ed.*, 2010, **49**, 8630–8634.
26 R. Vaidhyanathan, D. Bradshaw, J. N. Rebilly, J. P. Barrio, J. A. Gould, N. G. Berry and M. J. Rosseinsky, *Angew. Chem., Int. Ed.*, 2006, **45**, 6495–6499.
27 J. Rabone, Y. F. Yue, S. Y. Chong, K. C. Stylianou, J. Basca, D. Bradshaw, G. R. Darling, N. G. Berry, Y. Z. Khimyak, A. Y. Ganin, P. Wiper, J. B. Claridge and M. J. Rosseinsky, *Science*, 2010, **329**, 1053–1058.
28 J. An, S. J. Geib and N. L. Rosi, *J. Am. Chem. Soc.*, 2010, **132**, 38–39.
29 Y. Rachuri, J. F. Kurisingal, R. K. Chitumalla, S. Vuppala, Y. Gu, J. Jang, Y. Choe, E. Suresh and D. W. Park, *Inorg. Chem.*, 2019, **58**, 11389–11403.
30 J. An, S. J. Geib and N. L. Rosi, *J. Am. Chem. Soc.*, 2009, **131**, 8376–8377.
31 H. Hayashi, A. P. Côté, H. Furukawa, M. O'Keeffe and O. M. Yaghi, *Nat. Mater.*, 2007, **6**, 501–506.
32 J. Kahr, J. P. S. Mowat, A. M. Z. Slawin, R. E. Morris, D. Fairen-Jimenez and P. A. Wright, *Chem. Commun.*, 2012, **48**, 6690–6692.
33 L. Longley, N. Li, F. Wei and T. D. Bennett, *R. Soc. Open Sci.*, 2017, **4**, 171355.
34 K. M. Z. Hossain, U. Patel and I. Ahmed, *Prog. Biomater.*, 2015, **4**, 1–19.
35 I. Ahmed, M. Lewis, I. Olsen and J. C. Knowles, *Biomaterials*, 2004, **25**, 491–499.
36 A. M. Bumstead, M. L. Rios Gomez, M. F. Thorne, A. F. Sapnik, L. Longley, J. M. Tuffnell, D. S. Keeble, D. A. Keen and T. D. Bennett, *CrystEngComm*, 2020, **22**, 3627–3637.
37 M. F. Thorne, A. F. Sapnik, L. N. McHugh, A. M. Bumstead, C. Castillo-Blas, D. S. Keeble, M. Diaz Lopez, P. A. Chater, D. A. Keen and T. D. Bennett, *Chem. Commun.*, 2021, **57**, 9272–9275.
38 L. Xiang, L. Sheng, C. Wang, L. Zhang, Y. Pan and Y. Li, *Adv. Mater.*, 2017, **29**, 1–8.
39 M. Liu, R. D. McGillicuddy, H. Vuong, S. Tao, A. H. Slavney, M. I. Gonzalez, S. J. L. Billinge and J. A. Mason, *J. Am. Chem. Soc.*, 2021, **143**, 2801–2811.
40 P. G. Debenedetti and F. H. Stillinger, *Nature*, 2001, **410**, 259–267.
41 J. Yang, Y.-B. Zhang, Q. Liu, C. A. Trickett, E. Gutiérrez-Puebla, M. Á. Monge, H. Cong, A. Aldossary, H. Deng and O. M. Yaghi, *J. Am. Chem. Soc.*, 2017, **139**, 6448–6455.